Acta Crystallographica Section B
Structural Science
ISSN 0108-7681

Atomic and domain structure of the low-temperature phase of barium metagermanate ($BaGeO_3$)

Daniel Maria Többens,[a]* Volker Kahlenberg,[a] Christian Gspan[b] and Gerald Kothleitner[b]

[a]Institute of Mineralogy and Petrography, University of Innsbruck, Innrain 52, A-6020 Innsbruck, Austria, and [b]Research Institute for Electron Microscopy, Graz University of Technology, Steyrergasse 17, A-8010 Graz, Austria

Correspondence e-mail: daniel.toebbens@uibk.ac.at

Received 6 June 2006
Accepted 25 September 2006

The crystal structure of the low-temperature form of barium metagermanate ($BaGeO_3$) has been determined from laboratory X-ray powder diffraction data collected at 298.5 (5) K. The structure was found to consist of alternating layers of Ba cations and $[GeO_3]_3$ rings, and is closely related to pseudo-wollastonite. The rings show a twofold positional disorder owing to stacking faults. The stacking is not random, but can be rationalized by a twinning mechanism mapping the two non-congruent enantiomorphic polytypes of the structure onto each other. This model also explains the diffuse scattering and twinning observed in SAED and HRTEM, as well as the size and strain-like broadening effects found in the XRPD pattern.

1. Introduction

Over the last 50 years, the phase relationships (Shimizu *et al.*, 1970; Ozima *et al.*, 1982; Mikirticheva *et al.*, 2001; Shitova *et al.*, 2003) and the crystal chemistry (Jeffery & Heller, 1953; Liebau, 1960; Hilmer, 1962, 1963; Dornberger-Schiff, 1962; Nadezhina *et al.*, 1981*a*,*b*; Nishi, 1997; Yang & Prewitt, 1999) of oxo-silicates and germanates with the general composition ABO_3 (A: Ca, Sr, Ba; B: Si, Ge) have been studied intensively. For the silicate compounds this interest can also be explained by their importance in materials science and earth science. The α-modification of $CaSiO_3$ (pseudo-wollastonite), for example, is commonly found in slags and cements (Taylor, 1997). On the other hand, wollastonite or β-$CaSiO_3$ is also an important rock-forming mineral occurring in contact metamorphic rocks (Deer *et al.*, 1992). The germanates have been frequently used as convenient high-pressure model substances for the corresponding silicates on account of their lower transition pressures. A further interesting aspect of these materials is the existence of a complex polymorphism. In contrast to their comparatively simple chemistry, for most of the double oxides corresponding to the bulk composition mentioned above, at least two different modifications are known to exist at ambient pressure.

In the case of $BaGeO_3$, two different polymorphs have been reported. The so-called 'low-temperature' (LT) phase is the stable form at ambient conditions. Upon heating, LT-$BaGeO_3$ undergoes a first-order phase transition at *ca* 1423 K and transforms into the high-temperature (HT) modification. Unfortunately, in the literature usage of the Greek letters α and β for the designation of the two forms is not unique. Nevertheless, in most cases the designation α-$BaGeO_3$ corresponds to the LT form. The transformation is reversible and exhibits a pronounced thermal hysteresis. By rapid quenching the HT form can be readily preserved to room temperature. However, the metastable formation of HT-

Table 1
Experimental conditions and Rietveld analysis.

Instrument geometry	STOE symmetric transmission
Radiation type, source	X-ray, Cu $K\alpha_1$
Generator settings	40 kV, 40 mA
Discriminator	Primary beam, curved Ge(111) monochromator
Detector	Linear PSD, 6° width
Effective $\mu \cdot t$	2.3
Data collection temperature (K)	298.5 (5)
Range in 2θ (°)	2.0–130
PSD step size (°)	0.1, 8 × 20 s per step
Internal integration step size (°)	0.01
Space group	$C12/c1$
Chemical composition	$BaGeO_3$, $Z = 12$
No. of contributing reflections	942 total, 240 effective
No. of structural parameters	31
No. of other parameters	31
No. of restraints	12
R_{wp}, R_{exp}, R_{Bragg}	0.0427, 0.0316, 0.0454
Bérar factor	2.7

$BaGeO_3$ at *ca* 932 K has been also reported when an amorphous starting material prepared by the hydrolysis of barium and germanium alkoxides (Yamaguchi *et al.*, 1983) is used. The crystal structure of the HT form has been known for a long time (Hilmer, 1962). It belongs to the group of chain structures with $[Ge_2O_6]$-*zweier* single chains. For the LT modification, no structural data are available. Although several authors proposed a 'pseudo-wollastonite' structure model with tetrahedral rings, no structural characterization has been performed so far. The recent volume of the PDF-4 database contains an indexed powder pattern (entry No. 00-030-0127) of the LT phase. However, the reported figures-of-merit for the indexing clearly indicate that the given hexagonal unit cell with $a = 7.59$ and $c = 10.79$ Å is not correct. The aim of the present investigation was to elucidate the crystal structure of LT-$BaGeO_3$ in more detail. Since the first-order phase transition at 1423 K precludes the preparation of single crystals of the LT phase from slow cooling of the melt, we finally decided to use polycrystalline material for the structure determination based on high-resolution laboratory X-ray powder diffraction and electron microscopy.

2. Experimental

2.1. Sample preparation

A polycrystalline sample of $BaGeO_3$ was prepared by solid-state reactions using $BaCO_3$ (Sigma-Aldrich, for electronic purposes) and GeO_2 (Alfa Aesar, technical grade) as starting materials. A stoichiometric mixture of the reagents (1 g) was carefully homogenized in an agate mortar and subsequently pressed into discs. The discs confined in open 50 ml platinum crucibles were slowly heated from room temperature to 1323 K in a resistance-heated furnace held at this temperature for 48 h and finally quenched. The firing procedure was repeated twice. A first inspection of the synthesis product by X-ray powder diffraction revealed that the powder pattern corresponds to that reported for LT-$BaGeO_3$.

2.2. X-ray powder diffraction

X-ray powder diffraction data for detailed structural investigations have been collected on a Stoe Stadi MP diffractometer in symmetric transmission geometry using a circular sample of 8 mm diameter. A linear position-sensitive detector with a 6° detector range and Cu $K\alpha_1$ radiation from an asymmetric Ge(111) monochromator were used to measure a diffraction angle range of 2–130° with a total measuring time of 57 h. The experimental temperature was 298.5 (5) K. The absorption correction factor $\mu t = 2.3$ was experimentally determined from the intensity loss of the primary beam. For details of the diffraction experiment see Table 1.[1]

2.3. Electron microscopy

For the electron microscopy investigations the sample was spread out over a glass carrier and then transferred onto a TEM grid by dipping a holey carbon-film covered copper mesh into the powder, to ensure that the native structure remained unaltered. To avoid degradation of the sample during the measurement, the specimen was mounted into a cryo-specimen TEM holder, which was cooled to liquid nitrogen temperature. Electron microscopic data were obtained on a FEI TECNAI field emission microscope, operated at 200 kV primary energy. The selected-area electron diffraction patterns (SAED) were taken using a 10 µm aperture, selecting an area with a diameter of *ca* 430 nm. For the acquisition of the pattern, a camera length of 468 mm, measured relative to the CCD plane, was chosen and the sample was oriented towards a low-index zone, namely along the [010] axis by observing the corresponding Kikuchi maps. For diffraction the smallest condenser aperture of 50 µm was selected, whereas for phase-contrast imaging a 100 µm condenser and a 100 µm objective aperture were chosen. The phase-contrast high-resolution TEM images (HRTEM) have been energy-filtered using a Gatan Imaging Filter by taking solely the elastic signal at magnifications of 280 and 400 kx with respect to the CCD. All images were acquired on a Gatan UltraScan CCD camera, consisting of 2kx2k pixels in dark-subtracted and gain-normalized mode, and subsequent image processing was carried out using *DigitalMicrograph* software (Gatan Inc., 2003).

3. Structure solution and refinement

Peak positions for unit-cell determination were obtained by profile-fitting using the program *WinXPow* (Stoe, 2004). Indexing of the reflections was carried out with the *Crysfire* suite (Shirley, 2002) in combination with *Chekcell* (Laugier & Bochu, 2002). First attempts to index all reflections up to 80° directly did not give any useful results. However, focusing on

[1] Supplementary data for this paper are available from the IUCr electronic archives (Reference: WS5051). Services for accessing these data are described at the back of the journal.

the strong reflections only led to a hexagonal cell with $a = 4.40$, $c = 10.84$ Å. A search for the possible supercells using the Truecell algorithm implemented in Chekcell gave, among others, a monoclinic unit cell with lattice parameters of $a = 13.19$, $b = 7.62$, $c = 11.70$ Å, $\beta = 112.1^\circ$. The monoclinic and the hexagonal cell are related according to the following transformation matrix: (330), (1$\bar{1}$0), ($\bar{1}\bar{1}$1). Systematic extinctions for this cell were compatible with the space group $C2/c$. Subsequently, a LeBail-type profile-matching based on the monoclinic cell was performed with the program *FullProf* (Rodríguez-Carvajal, 2005) using Thompson–Cox–Hastings pseudo-Voigt functions and an asymmetry correction as proposed by Finger *et al.* (1994) for modelling the peak shape. The agreement between observed and calculated step intensities was very good, resulting in residuals of $R_{wp} = 0.0351$ and $\chi^2 = 1.21$. It became obvious during the later stages of the refinement that some anisotropic broadening had to be considered. This was taken into account by refining simultaneously uniaxial models for size and strain broadening; the details are described in the respective paragraphs. Two very broad peaks at 13.9 and 36.2° probably result from some small contribution of an amorphous phase. They have been treated as part of the background, which was described by linear interpolation between points with no- or low-peak intensity contributions.

The derived unit cell carries a striking resemblance to that of the well known structure of $SrGeO_3$ (Nishi, 1997), pointing to a structural relationship. In this compound, layers of strontium alternate with layers containing ternary Ge_3O_9 rings. Originally, interest in the structure of $SrGeO_3$ was sparked by the fact that it is isostructural to pseudo-wollastonite (Dornberger-Schiff, 1962; Hilmer, 1963). This observation compares well with earlier speculations on the structure of LT-$BaGeO_3$.

To test this hypothesis, a Rietveld refinement was performed with the program *FullProf* (Rodríguez-Carvajal, 2005) using the same profile models as for the LeBail profile-matching and the atomic coordinates of $SrGeO_3$ as a starting point for the structure of $BaGeO_3$. The resulting fit, however, was not fully satisfactory, with residuals of $R_{wp} = 0.0849$, $\chi^2 = 7.22$, $R_{Bragg} = 0.109$. Obviously, the model based on the structure of $SrGeO_3$, while not entirely wrong, was also not correct. The problem was found to be the position of the Ge_3O_9 rings: in the structure of $SrGeO_3$, the centres of the Ge_3O_9 rings are located on Wyckoff site 4(*e*): (0,*y*,1/4) with $y \simeq 0.58$. Occupation of this position places a single ring in the centre of a trigonal prism formed by six Sr cations. However, from a structural point of view there is an almost equivalent possible position for the rings at $x \simeq 2/3$, $y \simeq 0.58$, $y \simeq \frac{1}{4}$ [Wyckoff-site 8(*f*)], having the same environment for the alkaline earth cations. Locating the Ge_3O_9 groups on this position results in a twofold disordered distribution of the rings (Fig. 1). In $SrGeO_3$ this prism is not occupied. In the next step we investigated if this position could be a potential host for the rings in the barium compound. After introducing this structural modification the refinement was considerably improved and converged smoothly to final residuals of $R_{wp} = 0.0427$, $\chi^2 = 1.83$, $R_{Bragg} = 0.0454$ (Fig. 2). Atomic form factors in their respective valence state (Ba^{2+}, Ge^{4+}, O^{2-}) and an overall isotropic Debye–Waller factor were used. The experimentally determined absorption correction was applied to the data using the built-in function of the program for Stoe

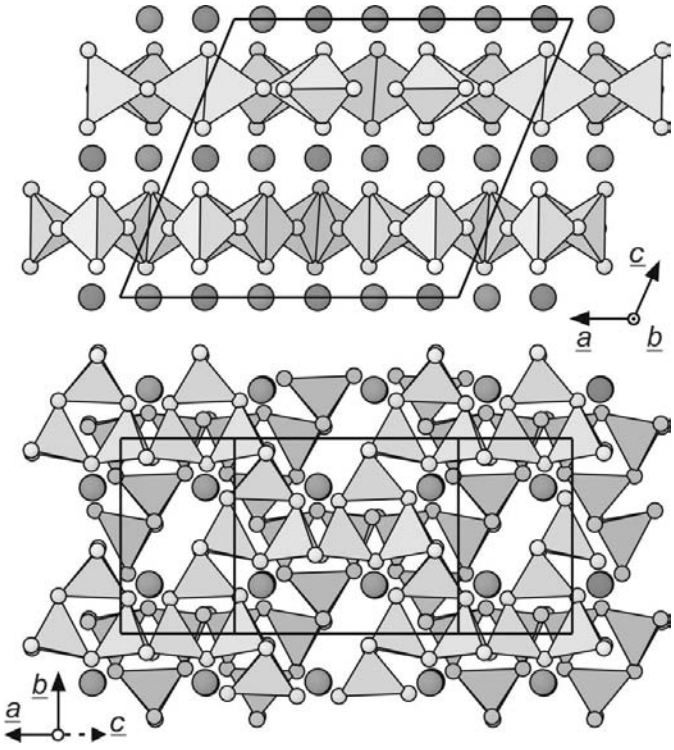

Figure 1
Crystal structure of $BaGeO_3$ (Ba: dark grey; O: light grey; GeO_4 tetrahedra: darker shades used as the depth cue). Note that the occupation of the Ge_3O_9 rings is only 50%. Structure drawings were prepared using *ATOMS* (Dowty, 1997).

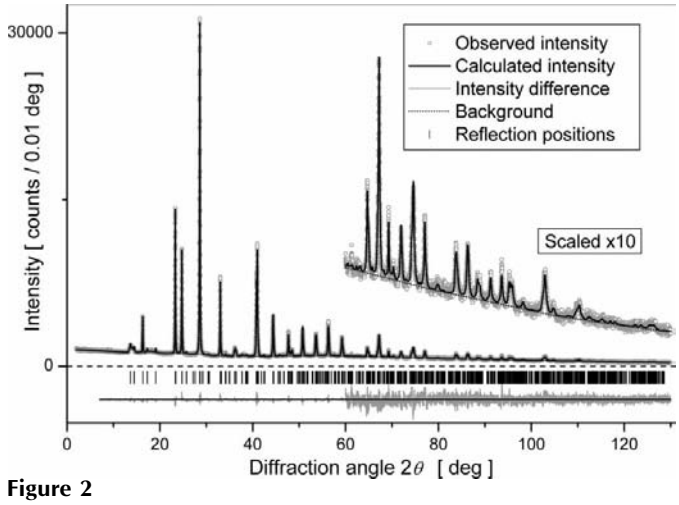

Figure 2
X-ray powder diffraction pattern of $BaGeO_3$ with Cu $K\alpha_1$ radiation. The high-angle region is shown scaled by a factor of 10 for clarity. Also given are the reflection positions of the main phase and the difference to the calculated pattern. Residuals of the Rietveld fitting are $R_{wp} = 0.042$, $\chi^2 = 1.8$, $R_{Bragg} = 0.045$. Note that at 13.9 and 36.2° two broad peaks appear, which probably result from some amorphous phase and have been modelled as part of the background.

Table 2
Structural parameters of $BaGeO_3$ in the space group $C2/c$.

All e.s.d.s should be multiplied by 2.7 for realistic uncertainties (Bérar & Lelann, 1991).

Atom	Wyckoff	x	y	z	Occupancy
Ba1	8(*f*)	0.0839 (3)	0.2521 (4)	0.5001 (6)	1.0
Ba2	4(*c*)	1/4	1/4	0.0	1.0
Ge1	8(*f*)	0.6591 (5)	0.8371 (7)	0.2505 (5)	0.5
Ge2	8(*f*)	0.7953 (5)	0.4653 (8)	0.2508 (5)	0.5
Ge3	8(*f*)	0.5429 (4)	0.4497 (7)	0.2508 (5)	0.5
O1	8(*f*)	0.5593 (15)	0.6811 (11)	0.2486 (34)	0.5
O2	8(*f*)	0.7634 (16)	0.6927 (12)	0.2471 (34)	0.5
O3	8(*f*)	0.6701 (21)	0.3738 (17)	0.2514 (61)	0.5
O4	8(*f*)	0.6052 (13)	0.9336 (22)	0.1082 (7)	1.0
O5	8(*f*)	0.6999 (16)	0.9374 (21)	0.3920 (7)	1.0
O6	8(*f*)	0.4572 (11)	0.4040 (34)	0.1055 (7)	1.0

a = 13.1895 (2), b = 7.6205 (1), c = 11.7170 (1) Å, β = 112.278 (1)°, B_{ov} = 0.73 (2) Å^2

transmission geometry. Soft distance constraints were applied to all Ge—O bonds; their target values were set to the ideal distance of 1.748 Å predicted from a bond-valence calculation (Brown & Altermatt, 1985) and were adjusted in weight so they affected the quality of the fit only slightly (R_{wp} without constraints was 0.0409). Details of the refinement are given in Table 1, structural parameters of the final model are summarized in Table 2.

3.1. Systematic verification of disorder

Since we could not exclude the possibility that the intuitively obtained distribution of the Ge_3O_9 rings is not entirely correct, several test runs were performed to locate rings within the structure of $BaGeO_3$ by simulated annealing using the program *FOX* (Favre-Nicolin & Černý, 2004). The starting model of the calculations was constructed as follows: Ba cations were attributed to the observed positions. Idealized flat Ge_3O_9 rings were constructed as rigid units with fixed Ge—O bond distances and tetrahedral angles. These units were placed parallel to the Ba layers around the centres of the prisms mentioned above. According to the orientation of the prisms, half of the rings were located in the orientation found in $SrGeO_3$ and the other half was inverted. With a total of 24 rings in the unit cell, the occupation for each ring was set to 1/6. Therefore, a structure with the highest possible disorder of Ge_3O_9 rings was created. Strong anti-bump restraints were applied for Ba—Ba, Ba—Ge and Ba—O distances. Structural parameters optimized by the simulated annealing process were the positions of the Ba cations and Ge_3O_9 units, the orientation and occupancy of the rings as well as an overall isotropic Debye–Waller factor. Only small displacement steps of up to 2.0 Å were used for the optimization. In order to deal with the anisotropic broadening of the reflections we decided not to use the raw profile for the simulated annealing, but rather to reconstruct the pattern from the peak positions and integrated intensities obtained from the LeBail extraction. For this purpose, pure Gaussian peaks with a constant FWHM of 0.13° were used. When convergence was reached, the optimization process was stopped and those rings showing (*a*) low occupancy or (*b*) severe superposition were removed. The simulated annealing was then re-started on the modified structure. The cycling was repeated until all reliable ring positions were located and subsequently, the final structure was refined with the Rietveld method. During the Rietveld analysis the Ge_3O_9 rings were subject to soft Ge—O distance restraints only. The sum of the occupation factors of the rings was constrained to keep the correct chemical bulk composition.

The procedure described above was applied to structure models in the space group $C2/c$, the maximal subgroups $P2_1/c$, $P2/c$, Cc and $C2$, as well as in Pc and $P1$. In summary, none of the lower-symmetry solutions resulted in a significantly better fit. The deviations from the $C2/c$ symmetry were negligible. Furthermore, the distribution of the ternary rings matched in all cases that of the final solution in $C2/c$ intuitively obtained from $SrGeO_3$. Application of the procedure to a structure model in the space group Cm, which is not a subgroup of $C2/c$, thus forcing a different ring distribution, did result in a significantly worse fit.

4. Anisotropic broadening of reflections

As mentioned previously, during the latter stages of the refinement it became obvious that some anisotropic broadening had to be considered, which especially affected reflections with the Miller index h close to zero. Refining a series of symmetry-adapted spherical harmonic functions (*FullProf* size model 15), following the method described by Järvinen (1993) for a $\cos^{-1}\theta$-dependent broadening of Lorentzian character, resulted in a significant reduction of the fit residuals. However, the resulting parameters were not physically meaningful. The model best suited to the problem, which gave physically realistic values and also resulted in the strongest reduction of the fit residuals (χ^2 = 1.82 for the final solution compared with 2.30 for the isotropic case), turned out to be a combination of two uniaxial effects. Size-like Lorentzian anisotropic broadening was refined using a model for platelet-coherent domains normal to [0,0,1] (*FullProf* size model 1). In addition, Gaussian broadening from the uniaxial microstrain (*FullProf* strain model 7) was refined. The strain axis was found to be approximately [1,0,−0.34], which is parallel to the **a** lattice vector. The resulting numerical values are an apparent size according to the Scherrer formula of 1543 (46) Å in the **c*** direction and an apparent maximum (upper limit) strain of 44.4 (4)‰ in the **a** direction. However, any interpretation of the broadening in terms of absolute values has to be considered as tentative. The instrument geometry chosen was selected to achieve the highest possible resolution, but in this geometry the instrumental function depends on the thickness of the sample. The corresponding parameters (U, W, X) had to be refined and, therefore, absolute values for the broadening

could not be obtained reliably. Furthermore, the pronounced hexagonal pseudo-symmetry of the material results in a severe overlap for the majority of strong reflections, resulting in a relatively high uncertainty of the finer details of the broadening. Nonetheless, the main characteristics of the anisotropy are evident.

5. Electron microscopy

SAED diffraction patterns (Figs. 3 and 4) could be completely indexed with the cell found from X-ray powder diffraction. Unfortunately, unambiguous assignment of indices is not possible owing to the pronounced pseudo-symmetry of the lattice. Because of this, important zone axes cannot be identified unequivocally, *i.e.* ⟨600⟩ and ⟨331⟩ are almost indistinguishable, as are ⟨020⟩ and ⟨−311⟩. Nonetheless, important features of the structure could be identified. The *C*-centring of the unit cell could also be confirmed from the systematic extinctions observed. The systematic extinction of reflections *h*0*l* with *l* = odd, related to the symmetry element c_y, was observed in some cases, but violated in others (*i.e.* Fig. 4). However, violation of systematic extinctions occurs frequently in electron diffraction and has to be analyzed carefully to draw the correct conclusions. In many cases, the observed area showed twinning (*i.e.* Fig. 3), the twin law of which can be described as the (100) mirror plane. Furthermore, pronounced diffuse streaks along **c*** are observed. This indicates disorder which is parallel to the **ab** plane and thus parallel to the layers of the structure. In no case was diffuse scattering observed in any other direction, confirming the strict two-dimensional character of the disorder. It should be noted that diffuse scattering does not appear in all rows along **c***, and was never observed in rows with *h* = 3*n*. HRTEM images of the structure clearly show the alternating layers of barium and germanium oxide (Fig. 4). Here also the disorder inside the layers can be observed. In some cases fully ordered domains can be observed which are inserted between disordered domains (Fig. 3). The domain borders in these cases are roughly parallel to the structural layers.

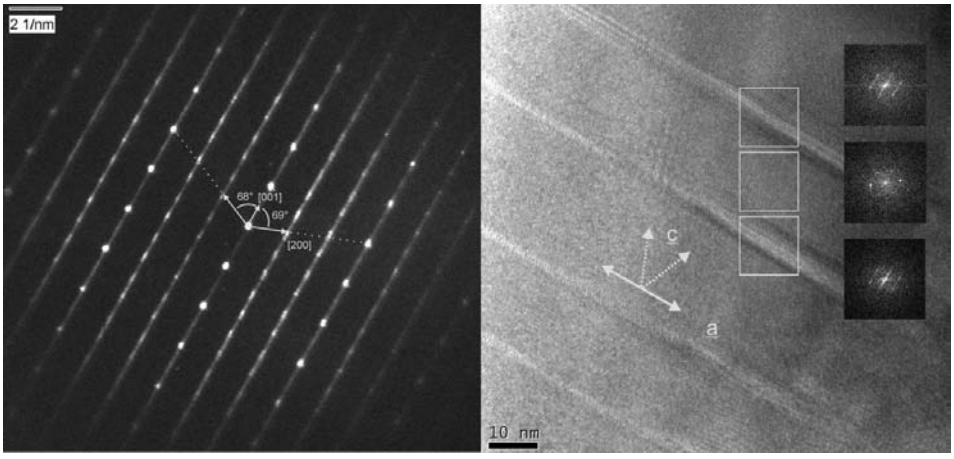

Figure 3
SAED diffraction pattern (left) and HRTEM picture (right) taken along the [010] zone axis of a twinned region. Insets in the HRTEM show diffraction patterns reconstructed from the indicated regions (squares); the directions of the basic lattice vectors are also indicated.

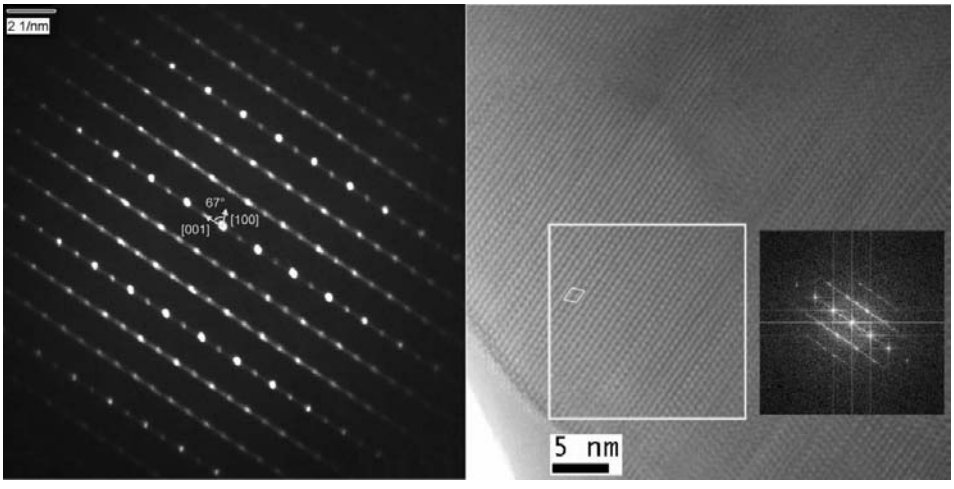

Figure 4
SAED diffraction pattern (left) and HRTEM picture (right) taken along the [010] zone axis of a highly disordered region. The insets show a SAED pattern reconstructed from the indicated region (square); the unit cell is also indicated.

Fig. 5 shows a simulated, well matching SAED pattern, calculated kinematically from the crystal structure by the commercial software package *JEMS*3.021 (Stadelmann, 1987). Besides the good overall agreement with the observed patterns of the same zone, it is especially noteworthy that weak reflections violating the condition *h*0*l*, *l* even, are predicted.

6. Discussion of the structure

The Ba cations in the structure form almost perfect triangular prisms with average Ba—Ba distances of 4.40 Å for the edges of the basal triangles, 5.42 Å for the joining edges and Ba—Ba—Ba angles of 90.0° within the joining faces. The maximum deviations from these average values are ± 0.03 Å, ± 0.003 Å and ± 0.3°, respectively. The basal faces of the prisms are parallel to the **ab** plane, forming close-packed layers of Ba cations at *z* = 0 and *z* = 0.5. Germanium is in a tetrahedral coordination by oxygen. Isolated

Table 3
Interatomic distances (Å) and angles (°) defining the Ge_3O_9 rings.

Soft distance constraints of 1.748 Å have been applied to all Ge—O bonds. All e.s.d.s should be multiplied by 2.7 for realistic uncertainties (Bérar & Lelann, 1991).

Ge1—O1	1.769 (19)	Ge2—O2	1.788 (12)	Ge3—O1	1.778 (10)
Ge1—O2	1.770 (20)	Ge2—O3	1.790 (40)	Ge3—O3	1.770 (40)
Ge1—O4	1.712 (11)	Ge2—O4	1.693 (10)	Ge3—O6	1.685 (10)
Ge1—O5	1.715 (11)	Ge2—O5	1.712 (14)	Ge3—O6′	1.720 (13)
O1—Ge1—O2	99.4 (20)	O2—Ge2—O3	99.7 (17)	O1—Ge3—O3	101.8 (18)
O1—Ge1—O4	104.3 (17)	O2—Ge2—O4	104.5 (12)	O1—Ge3—O6	103.4 (14)
O1—Ge1—O5	105.5 (14)	O2—Ge2—O5	101.2 (16)	O1—Ge3—O6′	104.9 (17)
O2—Ge1—O4	106.5 (14)	O3—Ge2—O4	108.5 (20)	O3—Ge3—O6	101.9 (19)
O2—Ge1—O5	109.7 (19)	O3—Ge2—O5	109.0 (40)	O3—Ge3—O6′	107.0 (40)
O4—Ge1—O5	127.7 (8)	O4—Ge2—O5	129.3 (9)	O6—Ge3—O6′	134.3 (9)
Ge1—O1—Ge3	139.5 (9)	Ge1—O2—Ge2	141.4 (10)	Ge2—O3—Ge3	138.1 (17)

Ge_3O_9 rings are formed by three corner-connected tetrahedra. The conformation of these rings is almost flat; the tetrahedral edges between the non-bridging O atoms (O4, O5, O6) are nearly perpendicular to the mean ring plane. Individual Ge—O bond distances and O—Ge—O angles show a considerable scatter. However, the values are in the normal range for oxogermanate structures. The Ge—O bond distances to the terminal O atoms are significantly shorter than the bridging Ge—O bonds ($\langle Ge-O_{term}\rangle$ = 1.71 ± 0.02 Å, $\langle Ge-O_{brid}\rangle$ = 1.78 ± 0.01 Å). The shortening of the non-bridging bond lengths compared with the bridging bond lengths results from the stronger attraction between O and Ge than between O and the Ba cations in the structure. The observed increase in bond angles at germanium for pairs of bonds containing only non-bridging oxygen (for details see Table 3) can be attributed to the necessity of avoiding Ba—O distances which are too short.

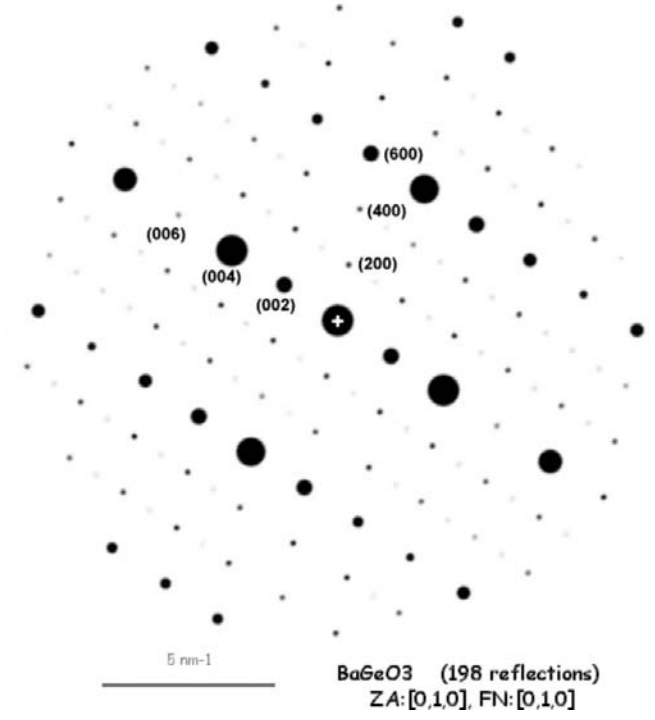

Figure 5
Simulated SAED diffraction pattern along the [010] zone axis.

However, for the discussion of the bond distances the influence of the positional disorder of the Ge_3O_9 rings has to be considered. Each position of the non-bridging atoms represents atoms belonging to two different rings, while all the other atomic positions in the model represent only one specific atom. These circumstances might influence the refined positions of the affected atoms and consequently, the respective interatomic distances and angles. Even so, the calculated values are crystallochemically reasonable.

Both symmetrically independent Ba cations are in a tenfold coordination with oxygen, with an average Ba—O distance of 2.83 Å and maximum deviations of ± 0.18 Å. The octahedral coordination of the ideal structure (Yamanaka & Mori, 1981), formed by the non-bridging oxygen atoms (O4, O5, O6), is still recognizable. However, the octahedral layers are strongly flattened in the direction normal to the **ab** plane, so that the thickness of the octahedral layer is reduced. Additionally, corner-connecting O atoms from four different adjacent ternary rings appear close to the Ba cations to complete the tenfold coordination. The occupancy of these O atoms is 0.5. Considering this disorder, the actual coordination number of barium is only eight.

As mentioned in the description of the structure determination process, the ternary rings are located in sheets parallel to the Ba layers. The centres of the rings coincide with the centres of the prisms formed by the Ba cations. One unit cell contains 24 prisms and only four rings in total. However, the respective dimensions of the prisms and rings place limitations on the simultaneous occupation of neighbouring prisms. Each prism shares its edges and faces joining the two contributing Ba layers with neighbouring prisms, sharing a common face with three neighbours and a common edge with nine more. If a prism is occupied by a ternary ring, a considerable part of each GeO_4 tetrahedron extends into those prisms having common joining faces. Owing to this, the occupation of any of the 12 neighbouring prisms by another ring would result in very short O—O distances. Therefore, within one layer there is just one structurally sound way to arrange the required number of ternary rings. The resulting pattern of ternary rings is fully ordered and all rings within one layer have the same basic orientation. This distribution is the one realised, *i.e.* in the fully ordered structure of $SrGeO_3$.

In the space group *C*2/*c* in each layer of the structure there are two symmetrically different prisms with the same orientation. One of these prisms has point symmetry 2, corresponding to the Wyckoff position 4(*e*) of its centre. The other prism is asymmetric with its centre at the Wyckoff position 8(*f*). While in the ordered structure of $SrGeO_3$ the ternary rings occupy the first type of prisms, in the structure discussed here only the latter ones are occupied. Owing to the higher multiplicity of this position the occupation factor of the prisms is only 0.5. The resulting disordered distribution of the ternary

rings is related to the ideal ordered distribution discussed before. It can be described as the superposition of two of these ideal distributions with the same orientation, but occupying different prisms. The exact nature of this disorder shall be discussed in the following.

6.1. Origins of the structural disorder

In their discussion of the structure and polytypes of pseudo-wollastonite (and the related $SrGeO_3$), Yamanaka & Mori (1981) show how these structures can be derived from the ideal layers described above by applying a number of different stacking operations. Besides the predominant four-layer polytype they also observed stacking-disordered polytypes of pseudo-wollastonite. This mechanism for disorder seems natural, since it does not require any disorder inside the layers. It also explains a number of the observations described above: The streaks of diffuse scattering along **c*** (which are observed in SAED) are explained by this model, **c*** being the direction normal to the layers in the structure and thus the stacking direction. Furthermore, stacking fault disorder is known to cause size-like broadening of Bragg reflections (Rodríguez-Carvajal, 2001). Layers which are fully ordered internally, but disordered in their stacking along the ***c**** direction, lead to the apparent shape observed here, a platelet normal to [001].

While stacking disorder by itself can explain the majority of the disorder-related observations, there are some additional considerations. In the observed distribution the ternary $[GeO_3]_3$ rings appear in only one out of two possible orientations and occupy only 2/3 of the positions which are compatible with this orientation, *i.e.* obviously the stacking is not completely random. There is, however, a plausible mechanism to explain the observed selection: following the terminology of Yamanaka & Mori (1981), $BaGeO_3$, like $SrGeO_3$, forms a so-called six-layer structure, in which the seventh layer is located just above the first layer along the stacking direction. The possible polytypes resulting from stacking of these layers with strictly ordered distributions of the ternary rings have been discussed extensively. In particular, for a resulting structure to have an inherent space-group symmetry of $C2/c$, there is only one distinct type. In this type, the symmetry element that maps the ternary rings of one layer of the structure onto the next one is the c_y glide plane. In accordance with the six-layer character of the structure, this symmetry element is associated with a shift of 1/2 of an intra-layer Ba—Ba distance, corresponding to 1/6 of the lattice parameter a. This type is the structure realised in $SrGeO_3$. There are, however, two non-congruent enantiomorphic polytypes of this structure. The disorder observed in the structure of $BaGeO_3$ can be described as the simultaneous appearance of both polytypes. If stacking of the layers does only allow for the formation of one of the two $C2/c$ polytypes, it follows directly that only the observed ring positions can be occupied.

The relation between the two $C2/c$ polytypes can be expressed by a twin mirror plane normal to **a**. The existence of these twins in macroscopic coherent domains can be seen directly in SAED. Furthermore, this twinning explains the observed microstrain along **a**, since it hinders the relaxation of any structure deformations in this direction, which the local ordering of the ternary rings might cause.

7. Conclusion

The crystal structure of the low-temperature form of barium metagermanate was found to be closely related to pseudo-wollastonite, consisting of alternating layers of Ba cations and $[GeO_3]_3$ rings Also, like pseudo-wollastonite, barium metagermanate shows stacking fault disorder, which here was shown to primarily affect the position and orientation of the $[GeO_3]_3$ rings. The stacking is not random, but can be rationalized by a twinning mechanism mapping the two non-congruent enantiomorphic polytypes of the structure onto each other. A more detailed description of the disorder could probably be derived from analysis of the diffuse scattering. However, this task would exceed the scope of this paper.

The authors thank P. Vulić and A. Kremenović for helpful discussions of the XRPD peak broadening.

References

Bérar, J.-F. & Lelann, P. (1991). *J. Appl. Cryst.* **24**, 1–5.
Brown, I. D. & Altermatt, D. (1985). *Acta Cryst.* B**41**, 244–247.
Deer, W. A., Howie, R. A. & Zussman, J. (1992). *An Introduction to the Rock-Forming Minerals*, 2nd ed. London: Longman.
Dornberger-Schiff, K. (1962). *Sov. Phys. Crystallogr.* **6**, 694–700.
Dowty, E. (1997). *ATOMS* for Windows, Version 5.1. Shape Software, Kingsport, Tennessee 37663, USA.
Favre-Nicolin, V. & Černý, R. (2004). *Z. Kristallogr.* **219**, 847–856.
Finger, L. W., Cox, D. E. & Jephcoat, A. P. (1994). *J. Appl. Cryst.* **27**, 892–900.
Gatan Inc. (2003). *DigitalMicrograph* 3.10.1, unpublished.
Hilmer, W. (1962). *Acta Cryst.* **15**, 1101–1105.
Hilmer, W. (1963). *Sov. Phys. Crystallogr.* **7**, 573–576.
Järvinen, M. (1993). *J. Appl. Cryst.* **26**, 525–531.
Jeffery, J. W. & Heller, L. (1953). *Acta Cryst.* **6**, 807–808.
Laugier, J. & Bochu, B. (2002). *LMGP Suite of Programs for the Interpretation of X-ray Experiment.* ENSP/Laboratoire des Matériaux et du Génie Physique, BP 46, 38042 Saint Martin d'Hères, France; http://www.inpg.Fr/LMGP/.
Liebau, F. (1960). *N. Jahrb. Mineral. Abh.* **94**, 1209–1222.
Mikirticheva, G. A., Shitova, V. I., Petrov, S. A, Grabovenko, L. Yu., Kuchaeva, S. K. & Grebenshchikov, R. G. (2001). *Russ. J. Appl. Chem.* **74**, 1270–1273.
Nadezhina, T. N., Pobedimskaya, E. A., Ilyukhin, V. V. & Belov, N. V. (1981*a*). *Sov. Phys. Crystallogr.* **26**, 27–32.
Nadezhina, T. N., Pobedimskaya, E. A., Ilyukhin, V. V. & Belov, N. V. (1981*b*). *Sov. Phys. Crystallogr.* **26**, 268–271.
Nishi, F. (1997). *Acta Cryst.* C**53**, 399–401.
Ozima, M., Susaki, J., Akimoto, S. & Shimizu, Y. (1982). *J. Solid State Chem.* **44**, 307–317.
Rodríguez-Carvajal, J. (2001). *An Introduction to the Program FullProf* 2000. Laboratoire Léon Brillouin (CEA-CNRS), CEA/Saclay, France.
Rodríguez-Carvajal, J. (2005). *FullProf*2k, Version 3.40. Laboratoire Léon Brillouin (CEA-CNRS), CEA/Saclay, France.
Shimizu, Y., Syono, Y. & Akimoto, S. (1970). *High Temp. High Press.* **2**, 113–120.

Shirley, R. (2002). *The Crysfire*2002 *System for Automatic Powder Indexing, User's Manual.* The Lattice Press: Guildford, Surrey, England.
Shitova, V. I., Mikirticheva, G. A., Petrov, S. A., Kuchaeva, S. K., Grabovenko, L. Yu. & Grebenshchikov, R. G. (2003). *Russ. J. General Chem.* **73**, 17–19.
Stadelmann, P. A. (1987). *Ultramicroscopy*, **21**, 131–146.
Stoe (2004). *WinXPow*2.10. Unpublished.
Taylor, H. W. F. (1997). *Cement Chemistry*. London: Thomas Telford.
Yamaguchi, O., Ki, M., Niimi, T. & Shimizu, K. (1983). *Polyhedron*, **2**, 1213–1216.
Yamanaka, T. & Mori, H. (1981). *Acta Cryst.* B**37**, 1010–1017.
Yang, H. & Prewitt, C. T. (1999). *Am. Mineral.* **84**, 929–932.